

Article

A New Mixed-Metal Phosphate as an Efficient Heterogeneous Catalyst for Knoevenagel Condensation Reaction

Avik Chowdhury [†], Sudip Bhattacharjee [†] , Sayantan Chongdar, Bhabani Malakar, Anindita Maity and Asim Bhaumik ^{*} 

School of Materials Sciences, Indian Association for the Cultivation of Science, 2A & 2B Raja S. C. Mullick Road, Jadavpur, Kolkata 700032, India; msac@iacs.res.in (A.C.); sudipb.hkc@gmail.com (S.B.); the.sayantan.97@gmail.com (S.C.); bhabanimalakr1997@gmail.com (B.M.); am.chem@chakdahacollege.ac.in (A.M.)

* Correspondence: msab@iacs.res.in

[†] These authors contributed equally to this work.

Abstract: The escalating demand for the cost-effective synthesis of valuable fine chemicals has fueled the search for sustainable heterogeneous catalysts. Among these catalytic reactions, Knoevenagel condensation has emerged as a very demanding reaction due to its involvement in the synthesis of new C–C bond formation. Porous metal phosphates have attracted significant attention in catalysis due to their unique surface properties. In this study, we report the synthesis of a novel porous magnesium aluminum phosphate (MALPO) material through a hydrothermal template-free approach. MALPO exhibited very promising specific surface area and hierarchical porosity. Moreover, the plate-like morphology of the material can enhance the exposure of the catalytic sites located at the surfaces, leading to enhanced catalytic activity. MALPO demonstrated excellent catalytic performance, yielding a series of Knoevenagel products with up to 99% yield. Notably, the catalyst displayed remarkable recyclability, retaining its structural integrity throughout multiple reaction cycles. The findings highlight the potential of porous mixed-metal phosphates, exemplified by MALPO, as sustainable and efficient base catalyst for the synthesis of value-added chemicals, contributing to the growing demand of the chemical industry. Further investigations are warranted to explore their catalytic potential in diverse chemical transformations and optimize their performance for large-scale operations.

Keywords: porous metal phosphate; heterogeneous catalysis; Knoevenagel condensation; base catalysis



Citation: Chowdhury, A.; Bhattacharjee, S.; Chongdar, S.; Malakar, B.; Maity, A.; Bhaumik, A. A New Mixed-Metal Phosphate as an Efficient Heterogeneous Catalyst for Knoevenagel Condensation Reaction. *Catalysts* **2023**, *13*, 1053. <https://doi.org/10.3390/catal13071053>

Academic Editors: Georgios Bamos, Athanasia Petala and Zacharias Frontistis

Received: 11 May 2023
Revised: 25 June 2023
Accepted: 26 June 2023
Published: 29 June 2023



Copyright: © 2023 by the authors. Licensee MDPI, Basel, Switzerland. This article is an open access article distributed under the terms and conditions of the Creative Commons Attribution (CC BY) license (<https://creativecommons.org/licenses/by/4.0/>).

1. Introduction

In the midst of a relentless surge for the green chemical synthesis, the chemical industry experiences an extraordinary upswing in the demand for suitable heterogeneous catalysts. Thus, the search for sustainable and cost-effective catalytic routes for synthesizing value-added chemicals has become a major concern for scientists worldwide. Knoevenagel condensation has been one of the most famous reactions in organic synthesis since its discovery (1890) [1] due to its massive importance in synthesizing valuable reactive organic building blocks [2,3]. In a typical Knoevenagel reaction a carbonyl compound reacts with active methylene groups to generate a new C–C bonds [4,5]. The reaction is found to be highly applicable for synthesizing various fine chemicals [6], hetero-Diels–Alder reactions [7,8], and carbocyclic as well as heterocyclic compounds with significant bio-active behavior [9]. Furthermore, the various kinds of intermediates, such as α , β -unsaturated esters; α -cyanocinnamates [10]; α , β -unsaturated nitriles; and cinnamic acid, involved in the Knoevenagel reaction are considered to be the major platform chemicals [11] for the pharmaceutical industry, the cosmetic industry, the production of perfumes, and the antihypertensive and polymer industries [12,13]. The Knoevenagel condensation reaction can proceed through an acid- or base-catalyzed pathway. So far, several attempts have been

made to understand the mechanistic pathway for this reaction. Initially, the methodologies were developed via homogeneous routes [14,15], but in the context of the long-term usage of catalysts, the homogeneous approach has serious shortcomings. In this context, the heterogeneous path is considered to be the most convenient due to the scope of the recyclability of catalyst, the ease of catalyst separation, and the cost-effectiveness of the process. Several heterogeneous catalysts displayed good performances in Knoevenagel condensation reactions such as the surfactant–mesoporous silica composite [16], functionalized MCM-41 [17], indium-doped AlMCM-41 [18], mesoporous carbon nitride [19], zeolites [20,21], porous organic polymers [22], metal–organic framework [2], phosphate complexes [23], coordination polymers [24], etc. However, use of these materials as catalysts may often lead to metal contamination in the final product.

Today, porous nanomaterials play a very crucial role in the field of heterogeneous catalysis due to their enhanced surface activity, pore size tunability, and ease of surface modifications. Previously, Gascon et al. reported AlMIL-53-NH₂ and IRMOF-3 in the Knoevenagel condensation of benzaldehyde with ethyl cyanoacetate [25]. On the other hand, Fischer et al. identified catalytic activities on several functionalized porous materials like Fe-MIL-101-NH₂, CAU-1-NH₂, and Al-MIL-101-NH₂ catalysts in the Knoevenagel condensation reaction of benzaldehyde with malononitrile and ethyl cyanoacetate [26]. Porous metal phosphates have emerged as a captivating class of materials [27] that has garnered significant interest within the realm of material science and engineering. These unique materials embody the fusion of advantageous properties exhibited by metals and phosphates, offering a broad spectrum of applications across diverse industries. Active catalytic sites in these porous metal phosphates are located at the surface of the interconnected pores [28] and can thus offer impressive catalytic activities.

Since the discovery of the aluminophosphate molecular sieve in 1982 by Wilson and coworkers [29], significant attention has been paid to the development of microporous aluminum phosphate molecular sieves [30–32]. Aluminum phosphate, a crystalline inorganic compound, is widely recognized for its diverse applications. Its similarities with zeolite make it a promising material in fields like gas separation [31], sensing, and heterogeneous catalysis. The framework of ALPO composed of AlO₄ and PO₄ moieties, due to the electronically neutral skeleton and the lack of sufficient acidic sites results in a very weak catalytic activity [33]. Over the past few years, significant strides have been made in the synthesis and characterization of porous metal phosphates. Advanced techniques, including solvothermal and hydrothermal methods [34,35], have been harnessed to produce materials with well-defined porosity and desirable properties. Moreover, researchers have focused their efforts on designing and modifying these materials to enhance their performance and expand their potential applications. Significant focus is directed towards the development of highly active ALPO materials, while considerable attention has been dedicated to the synthesis of ALPO materials incorporating different metal ions [36].

Over the past few decades, porous metal phosphates containing transition metals have garnered significant attention due to the high catalytic activity associated with the metal sites. The low-cost synthetic approach, as well as easiness in bulk synthesis, followed by significant reproducibility, make this class of materials a promising contender among the other members of the porous material family. Thus, immense effort is paying off in the fabrication of these materials, both in academia and industry. So far, a large number of different metal-incorporating aluminum phosphate catalysts have been reported. Acid properties can be significantly affected by introducing Ga, Si, and Co in the ALPO framework [37–39]. Generally, the synthesis of porous nanomaterials involves the use of structure directing agents (SDA) like amines or ionic/nonionic surfactants [38,40,41]. However, the removal of SDA can sometimes be very challenging, as the calcination process requires high temperatures, which often result in the collapse of the porous framework. Moreover, the emission of toxic gas during the calcination process is hazardous to nature. Thus, the template-free synthesis of surface-active porous metal phosphates has garnered significant attention in recent times. The scientific community is highly focused on the controlled

fabrication of crystalline porous frameworks with specific morphologies. This approach holds great promise due to the wide availability of active sites, resulting in remarkable outcomes. Researchers are actively exploring the synthetic process, recognizing its potential and the immense interest associated with it. Thus, the pursuit of morphology-controlled fabrication and the accessibility of active sites in transition metal phosphates have become a subject of immense scientific interest and investigation.

Herein, we report the synthesis of a new magnesium aluminum phosphate (MALPO) through a template-free hydrothermal synthesis approach. The resulting catalyst, MALPO, exhibited a good BET surface area and hierarchical porosity. The electron microscopic analysis revealed the plate-like morphology of the material, which facilitated enhanced surface exposure and improved catalytic activity. MALPO has been employed as a heterogeneous catalyst for the Knoevenagel condensation reaction under mild reaction conditions. Remarkably, MALPO demonstrated excellent catalytic performance, resulting in high yields of the desired products and significantly reduced reaction times. Moreover, the catalyst exhibited exceptional recyclability, retaining its structural integrity throughout multiple reaction cycles. These findings highlight significant potential of MALPO as a valuable catalyst for efficient and sustainable synthesis of organic value added chemicals. The further exploration and optimization of MALPO's catalytic properties are warranted to unlock its full potential for various chemical transformations and large-scale applications.

2. Results

Herein, we have synthesized porous magnesium aluminum phosphate (MALPO) using a template-free hydrothermal approach. The material was thoroughly characterized via different experimental tools. The bonding connectivity inside the material network was evaluated by carrying out a Fourier transform infrared (FTIR) spectroscopic analysis in a solid state by preparing the sample in the KBr pallet. The FTIR spectrum shown in Figure 1 indicates the presence of different bonding inside the material architecture. The peak at 3425 cm^{-1} could be attributed to the O–H stretching vibration [42]. On the other hand, peaks at the region of $1700\text{--}1550\text{ cm}^{-1}$ (1705 , 1655 , 1580 cm^{-1}) could be assigned to different H–O–H bending vibrations. The signals at 982 , 1017 , and 1053 cm^{-1} indicates the presence of phosphate groups. The 769 and 717 cm^{-1} peaks indicate the presence of metal oxygen bonds in the material [43,44].

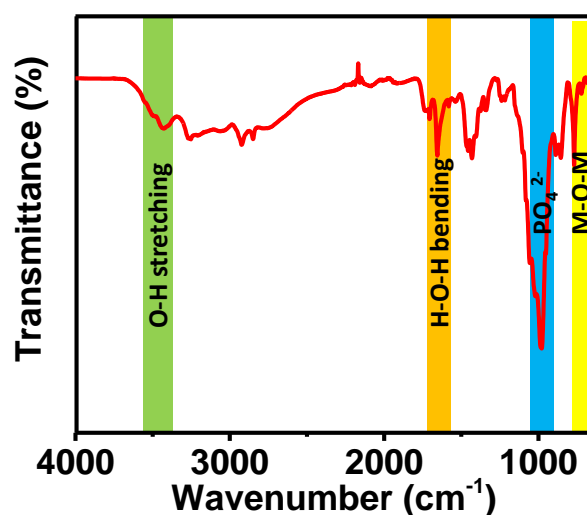


Figure 1. FTIR spectrum of MALPO.

The unit cell parameters and the crystalline phase of the MALPO was evaluated using the powder X-ray diffraction (PXRD) analysis. Prominent sharp crystalline peaks are observed at 10.08 , 11.04 , 12.77 , 13.21 , 18.96 , 21.12 , 23.13 , 25.29 , 26.72 , 28.79 , 30.56 , 31.88 , 35.48 , 37.53 , and 42.58 degrees of 2θ (Figure 2a). These aforementioned peaks were indexed

using the Expo2014 software [45], and these are assigned as 001, 101, 201, 210, 311, 30-2, 020, 021, 51-2, 711, 003, 91-1, 82-1, 812, and 31-4 planes, respectively (Table S1, ESI). The corresponding unit cell parameters of this phase of MALPO were $a = 27.652 \text{ \AA}$, $b = 7.683 \text{ \AA}$, $c = 8.866 \text{ \AA}$, $\alpha = 90.00^\circ$, $\beta = 98.56^\circ$, and $\gamma = 90.00^\circ$. The unit cell volume of MALPO was calculated as 1862.59 \AA^3 . The space group of this triclinic phase was assigned to $P1(1)$. A structural model of MALPO (Figure 2b) was developed using VESTA 4.5.0 software [46] in order to understand the connectivity and porosity in the framework. The refined simulated PXRD of the model was generated, which matched well with the experimental PXRD pattern with a low ESD value of 0.072.

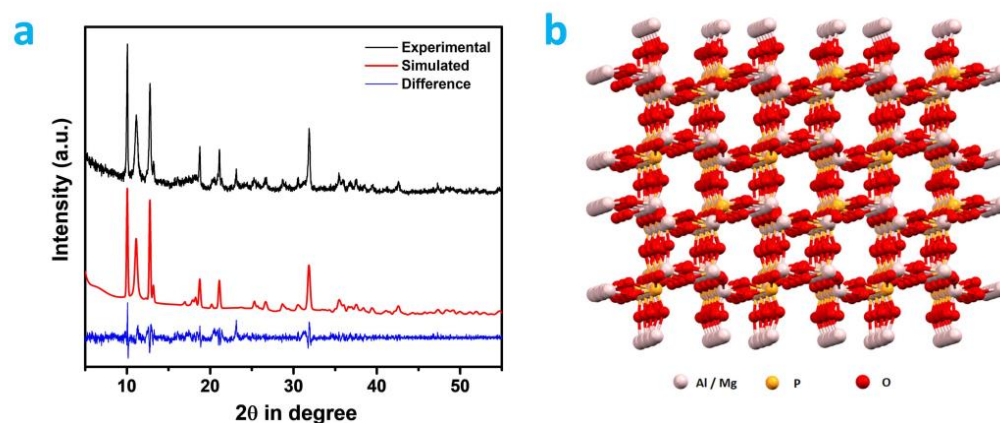


Figure 2. (a) Wide-angle powder XRD patterns: experimental (black), simulated (red), and difference (blue). (b) Ball and stick model of MALPO.

In order to investigate the porous nature of the as-prepared sample, nitrogen adsorption–desorption analysis was carried out at 77 K. The result is displayed in Figure 3. The isotherm indicated a mixture of type I and type IV isotherms, according to IUPAC convention [47]. A small rise in low pressure indicates the presence of microporosity and a steady rise in the N_2 uptake, along with a mild desorption hysteresis in the relative pressure region of 0.4 to 0.8 reflects the presence of mesoporosity. The pore size distribution, as observed in the inset Figure 3, obtained through non-local density functional theory analysis (NLDFT), reveals the presence of maximum pores with diameters of 1.6 to 2.6 nm. This finding suggests the existence of a dominant pore size within this range. The calculated BET surface area is measured to be $71 \text{ m}^2\text{g}^{-1}$. This N_2 sorption result indicates the significance of these specific pore sizes in the material, potentially influencing its properties and applications. Further investigation and characterization is warranted to explore the implications of this pore size distribution on the overall behavior and performance of the material.

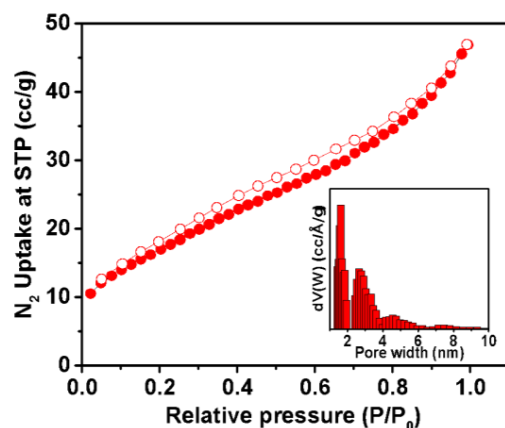


Figure 3. Nitrogen adsorption–desorption isotherm; pore size distribution curve (inset).

The MALPO's morphological characteristics were meticulously assessed utilizing ultra-high resolution transmission electron microscopy (UHR-TEM). The acquired TEM images, obtained at different resolutions, unveiled a compelling plate-like morphology exhibited by MALPO. Notably, Figure 4 vividly depicts the presence of rectangular sheets [48] in varying sizes, effectively highlighting the material's intricate structure. Remarkably, upon closer examination at a high resolution (Figure 4d), the TEM image uncovers the presence of crystalline fringes, aligning impeccably with the expected outcomes from its corresponding X-ray diffraction pattern. This observation strongly suggests the presence of a well-defined crystal lattice within the material, underscoring its inherent structural integrity. The identified two-dimensional (2D) morphological feature holds tremendous potential for enhanced surface activity [49], primarily attributable to the significantly augmented surface exposure that it offers. This unique characteristic opens up exciting prospects for applications where improved [50] surface reactivity and accessibility are critical factors.

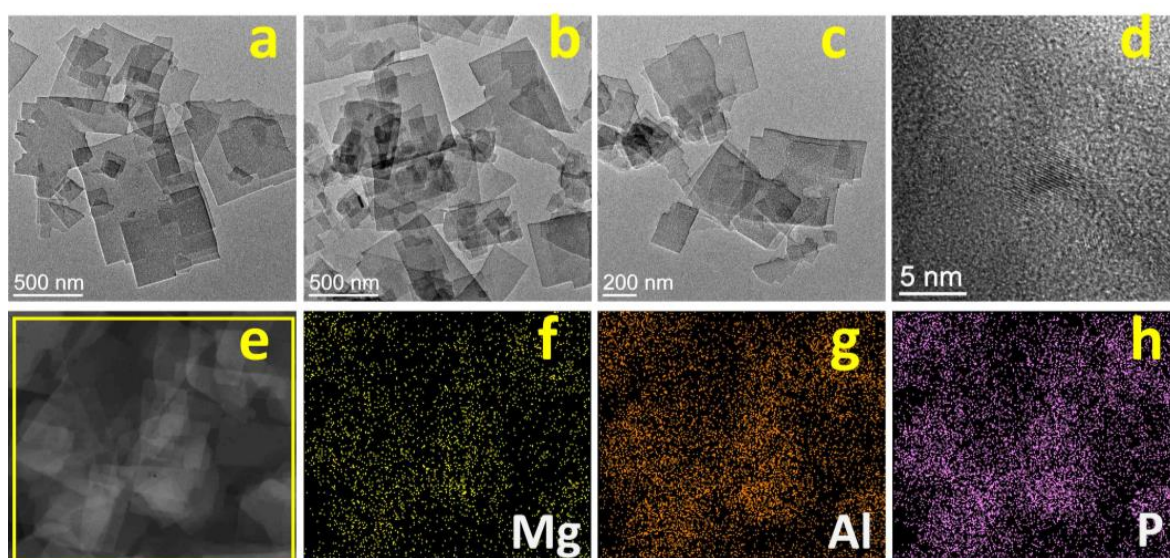


Figure 4. Transmission electron microscopy images of MALPO at different magnifications (a–d), selected area image under elemental mapping (e), elemental mapping of MALPO and the distribution of magnesium (Mg, (f)), aluminum (Al, (g)) and phosphorus (P, (h)).

In addition to the morphological evaluation, an elemental distribution (Figure 4f–h) analysis was performed using energy-dispersive X-ray spectroscopy (EDAX) on the TEM images. Notably, the results obtained demonstrate that a strikingly uniform presence of elements throughout MALPO. CO_2 -TPD analysis was carried out under an inert He gas flow, and the corresponding CO_2 desorption profile of MALPO is shown in Figure 5. As can be seen from this CO_2 -TPD profile, a broad CO_2 desorption peak with maxima at a very high temperature of 670°C can be observed. The presence of no significant CO_2 desorption peaks at lower temperatures suggests that CO_2 molecules are strongly bound at the MALPO surface. The observed total basicity was $3.15\ \mu\text{mol g}^{-1}$. On the other hand, to measure the surface acidity of MALPO, we performed acid–base titration (see the Supporting Information), which suggested a total acidity of $0.71\ \text{mmol g}^{-1}$. The presence of defect phosphate groups are responsible for this surface acidity in MALPO.

Catalytic Activity of MALPO

Knoevenagel condensation is a classical organic transformation in which an active methylene molecule reacts with a carbonyl compound to produce an α,β -conjugated enone. As these intermediates are extensively used in perfumes, polymers, fine chemicals, cosmetics, medicines, and pharmaceuticals, many research groups are concentrating on developing heterogeneous solid catalysts for this organic reaction to generate relevant products. Basic

or acidic nature-based catalysts are often used to carry out the condensation reaction, but this requires high reaction temperatures or microwave irradiation [51,52]. Although many catalytic systems have been reported for this reaction, it is very challenging to develop a catalyst which can promote this reaction without the formation of by-products due to the consecutive self-condensation and oligomerization reactions of the primary reaction product [53,54]. The type of catalyst used has a significant impact on product selectivity. In the presence of a Brønsted-base, it results in benzylidene malononitrile, while in presence of Lewis's acid, benzaldehyde reacts with ethanol solvent to produce the desired product (Figure 6). To investigate the catalytic activity of the MALPO, the Knoevenagel condensation reaction was performed by taking benzaldehyde and malononitrile as model substrates in ethanol as the solvent. The reaction yielded the desired benzylidene malononitrile through the activation of a methylene group followed by aldol condensation under the present experimental conditions. As previously discussed, ethanol is considered as the best solvent when compared to MeCN, benzene, toluene, and DCM; thus, we performed our reaction with ethanol [55]. Before confirming the catalytic activity, a blank test was performed without using catalyst, which did not provide the suitable results after 2 h of reaction (17% conversion) in ethanol at room temperature.

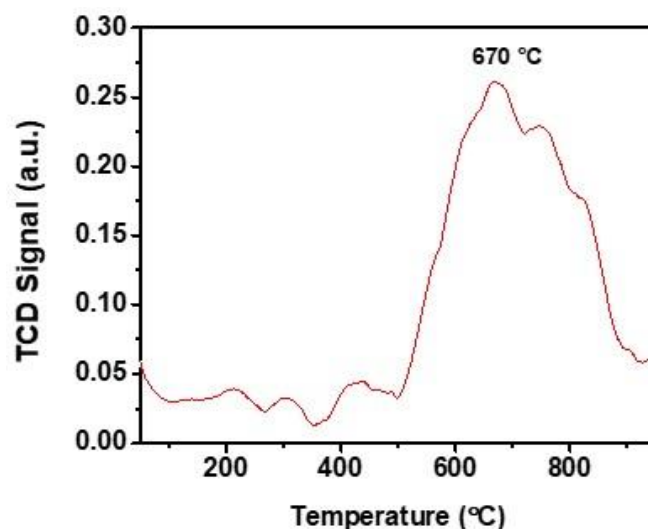


Figure 5. Temperature programmed desorption of CO₂ profile of MALPO in the temperature range 50–875 °C.

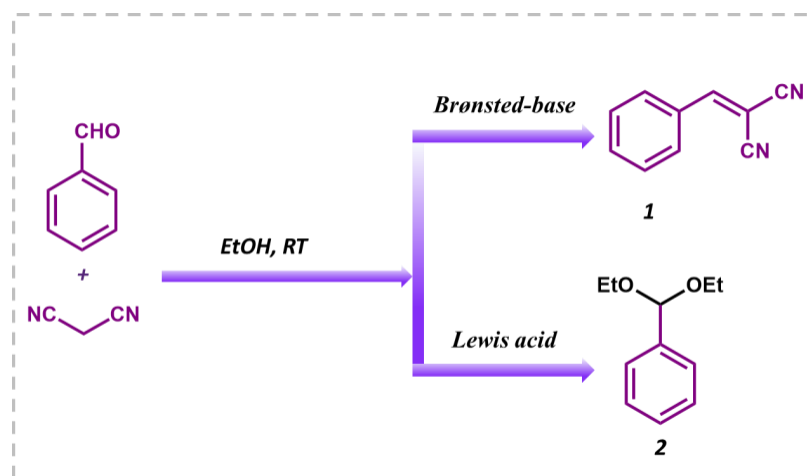


Figure 6. Knoevenagel condensation reaction between benzaldehyde and malononitrile in ethanol as the solvent to obtain benzylidene malononitrile (1) and the undesired by-product benzaldehyde diethyl acetal (2).

In the same experimental conditions, a 99% conversion of benzaldehyde was accomplished using MALPO in ethanol at room temperature after only 100 min. The results clearly reveal the contribution of catalysts towards the activation of this reaction. As we observed that the reaction proceeds smoothly in ethanol within 100 min, we further identified the actual required time for this conversion. Then, we performed the reaction at different time intervals, which is shown in Figure 7a, and while it was observed for 100 min, the reaction was completed within 60 min.

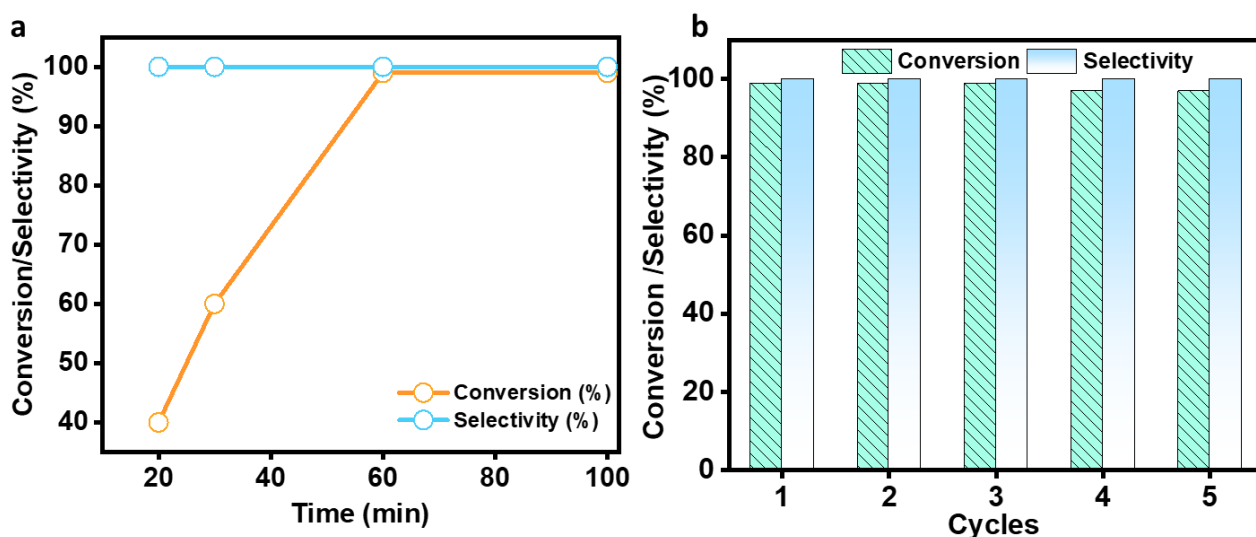


Figure 7. Conversion/selectivity plot with respect to the time (a) and the recyclability experiment (b).

To verify that the observed reaction was solely stimulated by a solid catalyst and not due to active sites leaching into the solution, a leaching experiment was conducted under identical conditions. Specifically, the benzaldehyde and malononitrile reaction was initiated in the presence of MALPO under the same circumstances. After 30 min, an aliquot was extracted from the reaction mixture and filtered in order to eliminate the solid catalyst, allowing the resulting solution to continue reacting for an additional 30 min. The outcomes of this leaching experiment are presented in Figure S1 of the Supplementary Materials, which clearly demonstrate that the reaction rate experienced a substantial reduction in the absence of the catalyst following the filtration step. These results indicate that the presence of MALPO exclusively catalyzes the reaction, without any active sites leaching from the solid catalyst into the solution. However, the slight increase in the conversion of benzaldehyde after the catalyst's removal may be attributed to the contribution from the blank reaction, as indicated.

Having observed that the MALPO catalyst achieves an impressive 99% conversion of benzaldehyde to benzylidene malononitrile at room temperature, further experimentation at higher temperatures was deemed unnecessary. Subsequently, upon successfully optimizing the catalytic performance of MALPO for the Knoevenagel reaction, the scope of substrates was expanded to include aromatic-substituted aldehydes (Figure 8, 1a–1e) and biomass-derived heterocyclic aldehydes (Figure 8, 1f). Notably, the catalyst demonstrated the efficient conversion of various substrates, including those with electron-withdrawing groups in the para position and furfural, yielding their corresponding derivatives with high efficiency. However, para-fluoro benzaldehyde (Figure 8, 1c) proved to be an exception, as it did not undergo conversion under the same reaction conditions. The catalyst was also probed for a different active methylene group, such as ethyl cyanoacetate with benzaldehyde (Scheme 1), which showed a 94% conversion (Figure S6, ESI) regarding the condensation reaction under refluxing conditions. These findings highlight the unique catalytic prowess of MALPO and its broad substrate compatibility, thereby showcasing its

potential for diverse synthetic applications, ranging from aromatic substituted aldehydes to biomass-derived heterocyclic aldehydes.

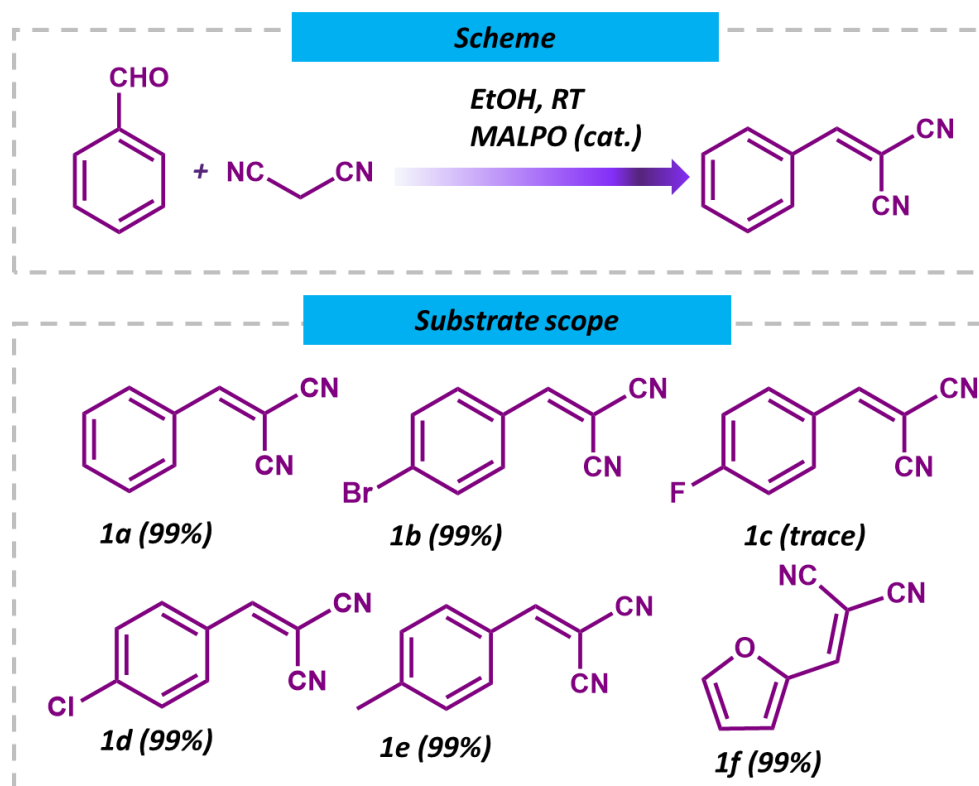
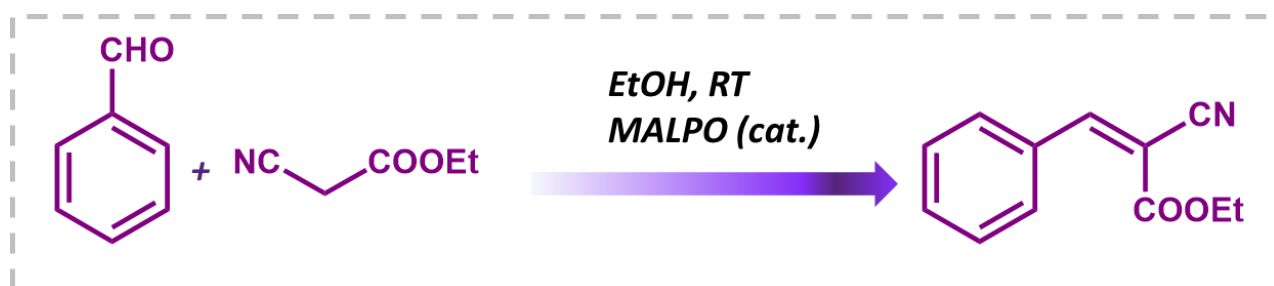


Figure 8. Scheme and substrate scopes and reaction conditions for the Knoevenagel condensation reactions for MALPO.

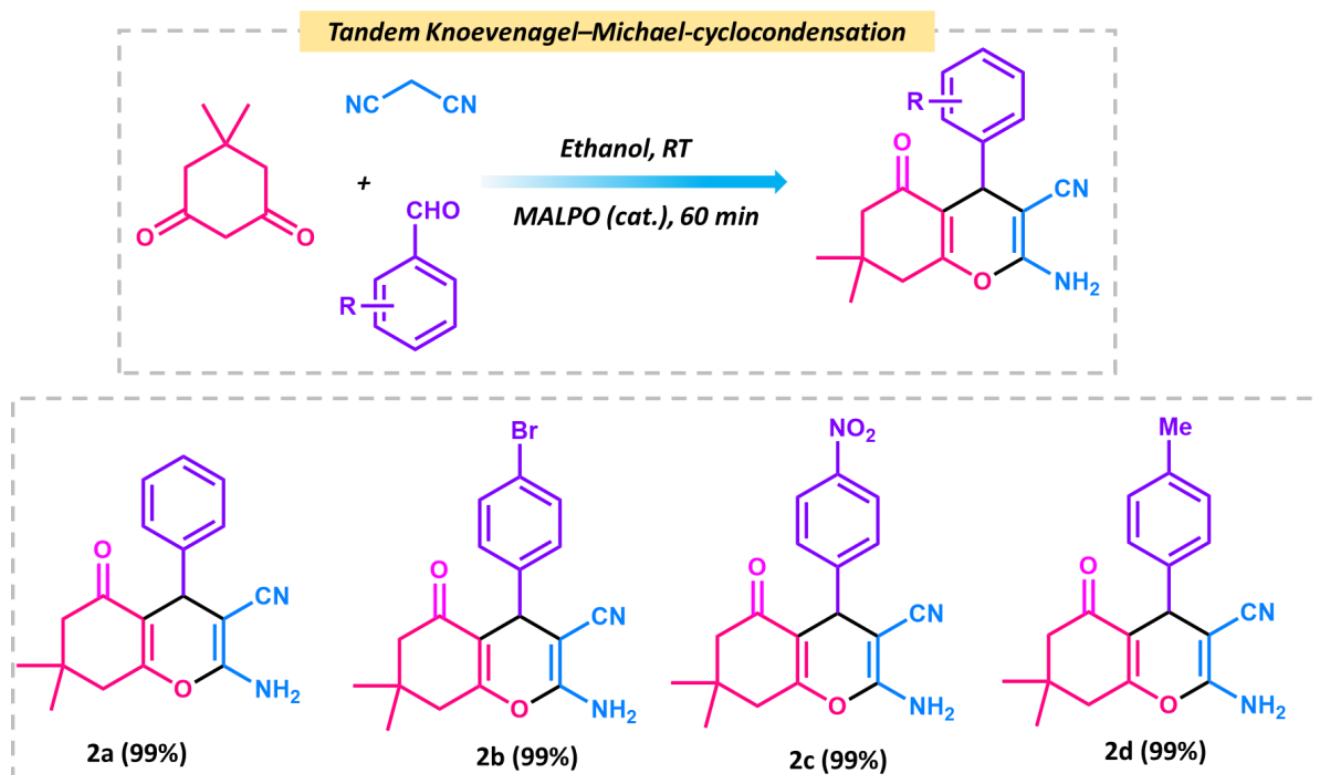


Scheme 1. Schematic representation of the Knoevenagel condensation of ethylcyanoacetate and benzaldehyde.

After the initial experiment, we ran a recyclability test for consecutive fourth cycle to verify the heterogeneity of the catalyst. The catalyst was collected after each cycle, properly washed with methanol, and activated at 120 °C for two hours to conduct the recyclability test. The catalyst was utilized for four successive cycles after it had been activated, and the conversion/selectivity plot is shown in Figure 7b. Up to the fourth cycle, no discernible difference in conversion or O_2 at acid–base paired sites on the catalyst surface that effectively catalyze the deprotonating aldol–dehydration processes was observed. The powdered X-ray diffraction pattern was taken after the fourth cycle (Figure S8, ESI) to assess the stability of the MALPO, and it reveals that there was no structural change. According to Figure 8a, the high catalytic activity of MALPO could be attributed to the basic sites, which promote the abstraction of the protons and activate the malononitrile. This active

methylene attacks the $-C=O$ bond of benzaldehyde, which further eliminate the water via aldol condensation, resulting in the final benzylidene malononitrile product.

After the Knoevenagel reaction, we further extended the procedure to produce tetrahydrobenzo[*b*]pyrans. This is a good example of tandem Knoevenagel–Michael cyclocondensation [56] reaction (Scheme 2). To perform the reaction, we chose malononitrile, aromatic aldehyde, and dimedone as model substrates in ethanol. The overall reaction was carried at room temperature, which resulted in a 99% conversion after 1 h of reaction. The reaction follows the same pathway, which follows the Knoevenagel in the first step and further reacts with dimedone to form the pyran derivative via cyclo condensation. The plausible mechanism is shown in Figure 9 In the first step, the MALPO catalyst activates the malononitrile to form the active methylene group, which reacts with the carbonyl group of the aldehyde to form the intermediate **I** via the removal of one molecule of H_2O . On the other hand, dimedone favors the enol form after tautomerization, which attacks the cyano-olefin compound **I** and which behave as a Michael acceptor to produce intermediate **II**. After the formation of intermediates **II**, it follows the cyclo-condensation via the bond shifting of $-C=O$ to the corresponding nitrile group to form intermediate **III**. This intermediate **III** gives the final product by abstracting protons from the reaction mixture. After the successful conversion of the pyran derivatives of benzaldehyde, we examined the catalytic activity on the substrate scope for *p*-bromo derivatives, which provide 99% conversion. *p*-nitro derivatives also give higher yields. From the above mentioned results, it can be concluded that the catalyst is very efficient for both types of Knoevenagel condensation reactions as well as Knoevenagel–Michael cyclo-condensation. The higher activity of MALPO is due to the presence of basic sites as well as acidic sites in the framework.



Scheme 2. Schematic representation of tandem Knoevenagel–Michael cyclocondensation reactions between dimedone, benzaldehyde, and malononitrile.

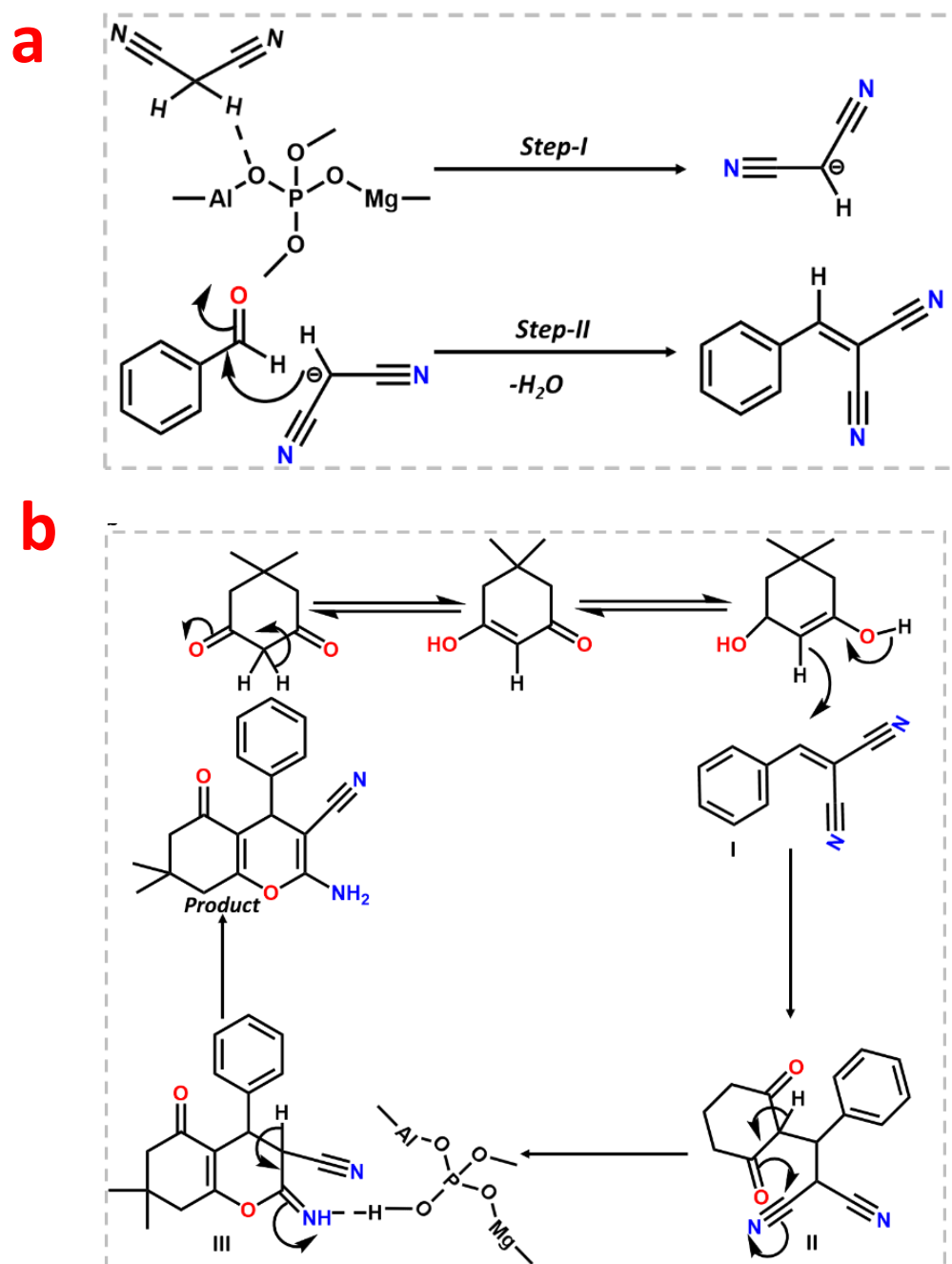


Figure 9. Probable mechanistic pathway for the Knoevenagel condensation reaction (a) and Knoevenagel–Michael cyclo-condensation (b).

3. Experimental

3.1. Characterizations

The bonding connectivity in the as-synthesized MALPO was analyzed using Fourier transform infrared (FTIR) spectroscopy and a Spectrum 100 spectrophotometer was used for the FTIR analysis (PerkinElmer, Cambridge, MA, USA). The crystalline nature of the phosphate materials was investigated using a Bruker D8 advance X-ray diffractometer, with Cu K α ($\lambda = 0.154$ nm) is used as an X-ray source (Bruker AXS, Karlsruhe, Germany). The surface area of the material was investigated by analyzing the Brunauer–Emmett–Teller (BET) surface through N₂ sorption analysis at 77 K using a Quantachrome Autosorb iQ surface area analyzer (Quantachrome Inc., Boynton Beach, FL, USA). In order to analyze

the data, the samples were activated in a hot air oven at 80 °C, followed by the gassing of the materials at 120 °C under continuous vacuum for 3 h. The pore size distribution was investigated using the non-local density functional theory (NLDFT) method. The morphological analysis of the materials was investigated by analyzing the images obtained from ultrahigh resolution transmission electron microscopy (UHR-TEM, JEOL, Tokyo, Japan). The conformation of the catalytic products was evaluated through nuclear magnetic resonance (NMR) spectroscopy using a Bruker Avance NMR spectrometer (Bruker AXS, Germany). The elemental distribution in the material architecture was analyzed using the elemental distribution images obtained through energy dispersive spectroscopy (EDS). The JEOL 2010 TEM (JEOL, Japan), operated at 200 kV, was utilized to capture ultrahigh-resolution transmission emission microscopy (UHR-TEM) images. For the TEM analysis, the sample was dispersed in methanol and then drop-cast onto a copper grid coated with a carbon polymer. For the temperature programmed desorption analysis of CO₂ (CO₂-TPD), the MALPO sample was activated at 250 °C under a He flow of 2 h. Then, after cooling the sample to room temperature, CO₂ was purged in the absence of a carrier gas flow for 30 min. Then, the sample temperature was raised in a step-wise manner with a heating rate of 10 °C min⁻¹. The desorbed CO₂ in the temperature range 50 to 875 °C was analyzed using a thermal conductivity detector fitted in a AMI-300 Chemisorption Analyzer (Altamira Instruments, Pittsburgh, PA, USA).

3.2. Chemicals

Magnesium nitrate hexahydrate (Mg(OH)₂ 6H₂O) (Spectrochem, Mumbai, India), and aluminum nitrate nonahydrate (Al(NO₃)₃ 9H₂O) and 28% ammonium hydroxide solutions were purchased from Merck, Bengaluru, India. Phosphoric acid (H₃PO₄) was purchased from TCI Chemicals, India. Benzaldehyde was purchased from Spectrochem, India, Furfural was purchased from Sigma-Aldrich (St. Louis, MO, USA), and 4-chlorobenzaldehyde and 4-bromobenzaldehyde were purchased from Merck, India. Dimedone and malononitrile were purchased from Sigma-Aldrich (USA). Of the solvents, ethanol was purchased from Bengal Chemicals (Kolkata, India); acetone and methanol were purchased from Finar Chemicals (Mumbai, India); and the NMR solvent CDCl₃ was purchased from Sigma-Aldrich (USA). All the reagents and solvents were used without any further purification.

3.3. Synthesis of MALP

Magnesium aluminum phosphate was synthesized via a typical hydrothermal [39] method. In the synthetic procedure, 1.54 g of phosphoric acid was dissolved in 10 mL of distilled water, 1.28 g of magnesium nitrate hexahydrate (Mg(NO₃)₂ 6H₂O; 0.005 mmol) and 1.87 g of aluminum nitrate nonahydrate (Al(NO₃)₃ 9H₂O, 0.005 mol) were separately placed in 5 mL distilled water. The metal precursor solutions were added simultaneously drop-wise, followed by the addition of 28% ammonium hydroxide solution (NH₄OH) in order to maintain a fixed pH of 7. The final solution was kept under vigorous stirring at room temperature for another 3 h. Finally, the solution was transferred to a stainless steel hydrothermal autoclave and kept static for 72 h at 180 °C in a hot air oven. After that, the white precipitate obtained was filtered, followed by washing with water, methanol, and tetrahydrofuran. Finally, the product was dried at 80 °C under vacuum. The material was then characterized using X-ray diffraction, Fourier-transform infrared spectroscopy, transmission electron microscopy, and nitrogen sorption isotherm analysis.

3.4. Catalytic Activity of MALPO

In order to conduct the catalytic activity test for the Knoevenagel condensation reaction, we carried out the following experiment. A total of 2 mmol of aromatic aldehydes was placed in a 50 mL round-bottomed flask. Then, 2 mmol of malononitrile was added, along with the pre-activated catalyst MALPO (10 mg), followed by the addition of 10 mL ethanol. The reaction mixture was then stirred at 400 rpm for the desired time and monitored via thin-layer chromatography (TLC). After the completion of the reaction, the reaction mixture

was filtered in order to separate out the solid catalyst. Thereafter, the liquid was dried under reduced pressure to obtain solid product. The conformation of the product was evaluated via ^1H NMR spectroscopy, where CDCl_3 was used as an NMR solvent.

3.5. Catalyst Recyclability Experiment

To assess the reusability of MALPO, we performed catalytic recyclability tests. After the catalytic performance, the MALPO material was recovered via filtration. The catalyst was then subjected to a series of washes using distilled water, methanol, and ethanol, followed by vacuum drying. This process regenerated the catalyst, allowing us to employ it for up to four consecutive catalytic cycles. Through this evaluation, we aimed to determine the extent to which MALPO could be reused as a catalyst, providing valuable insights into its potential for sustainable and efficient applications.

4. Conclusions

In summary, herein, we successfully synthesized porous magnesium aluminum mixed-metal phosphate MALPO using ortho phosphoric acid as a phosphate source. MALPO synthesized through a template free approach was found to possess a high specific surface area and a novel triclinic crystal structure. The basic sites present in the material make it a very efficient catalyst for the heterogeneous Knoevenagel condensation reaction. The series of substrates investigated result in excellent product yields of up to 99%. Furthermore, the recyclability test carried out demonstrated the enhanced recyclability of MALPO without any loss of structural integrity, which further concludes the long term applicability of the material towards heterogeneous catalysis. In conclusion, our investigation reveals that the novel mixed-metal phosphate material MALPO holds promise as a potential catalyst for facilitating the Knoevenagel condensation reaction. This observation suggests that MALPO exhibits favorable catalytic properties and could play a crucial role in meeting the growing demand for the synthesis of value-added chemicals, involving a new C–C bond. By offering enhanced catalytic efficiency, MALPO has the potential to contribute significantly to the development and validation of advanced chemical synthesis strategies in the near future. Further research and exploration are warranted in order to fully exploit the capabilities of MALPO and optimize its performance when catalyzing the Knoevenagel condensation reaction.

Supplementary Materials: The following supporting information can be downloaded at: <https://www.mdpi.com/article/10.3390/catal13071053/s1>, Figure S1: Leaching experiment indicating no leaching of active sites during catalysis, Figure S2: ^1H NMR of 2-benzylidenemalononitrile, Figure S3: ^1H NMR of 2-(4-chlorobenzylidene)malononitrile, Figure S4: ^1H NMR of 2-(furan-2-ylmethylene)malononitrile, Figure S5: ^1H NMR of 2-(4-bromobenzylidene)malononitrile, Figure S6: ^1H NMR of ethyl (*E*)-2-cyano-3-phenylacrylate, Figure S7: ^1H NMR of 2-amino-7,7-dimethyl-5-oxo-4-(*p*-tolyl)-5,6,7,8-tetrahydro-4(*H*-chromene-3-carbonitrile, Figure S8: PXRD pattern of recycled catalyst, Figure S9: (a) TEM image of MALPO; (b) distribution of oxygen in MALPO. Table S1: Indexing of triclinic phase of MALPO with space group P1.

Author Contributions: Experiments, investigation, and formal analysis were carried out by A.C. and S.B. S.C. was involved in the crystal structure analysis. B.M. and A.M. were involved in the formal analysis of the catalysts and products. A.B. provided the resources, investigation, and overall supervision of this project. A.C. wrote the draft manuscript with the help of A.B. All authors have read and agreed to the published version of the manuscript.

Funding: A.C. would like to thank CSIR, New Delhi, for the Senior Research Fellowship. S.B. would like to thank IGSTC, New Delhi, for the Senior Research Fellowship. B.M. would like to thank UGC, New Delhi, for the Junior Research Fellowship. A.B. would like to acknowledge DST-SERB, New Delhi, for the core research grant (project no. CRG/2022/002812).

Data Availability Statement: Not applicable.

Acknowledgments: Authors would like to thank Keshab Maikup for helpful discussion.

Conflicts of Interest: The authors have no conflict to declare.

References

1. Knoevenagel, E. Condensation von Malonsäure mit aromatischen Aldehyden durch Ammoniak und Amine. *Ber. Dtsch. Chem. Ges.* **1898**, *31*, 2596–2619. [[CrossRef](#)]
2. Zhu, L.; Liu, X.Q.; Jiang, H.L.; Sun, L.B. Metal-Organic Frameworks for Heterogeneous Basic Catalysis. *Chem. Rev.* **2017**, *117*, 8129–8176. [[CrossRef](#)] [[PubMed](#)]
3. Jing, Y.; Meng, J.; Liu, Y.; Wan, J.P. Direct Three-Component Synthesis of α -Cyano Acrylates Involving Cascade Knoevenagel Reaction and Esterification. *Chin. J. Chem.* **2015**, *33*, 1194–1198. [[CrossRef](#)]
4. Jones, G. *Organic Reactions*; Wiley: New York, NY, USA, 1967; Volume 15, pp. 204–599.
5. Tietze, L.F.; Beifuss, U.; Trost, B.M.; Fleming, I. *An Efficient, Base-Catalyzed, Aqueous Knoevenagel Condensation for the Undergraduate Laboratory*; Pergamon Press: Oxford, UK, 1991; Volume 2, pp. 341–394.
6. Freeman, F. Properties and Reactions of Ylidene malononitriles. *Chem. Rev.* **1981**, *80*, 329–350. [[CrossRef](#)]
7. Mondal, J.; Modak, A.; Bhaumik, A. Highly efficient mesoporous base catalyzed Knoevenagel condensation of different aromatic aldehydes with malononitrile and subsequent noncatalytic Diels-Alder reactions. *J. Mol. Catal. A Chem.* **2011**, *335*, 236–241. [[CrossRef](#)]
8. Borah, H.N.; Deb, M.L.; Boruah, R.C.; Bhuyan, P.J. Stereoselective intramolecular hetero Diels–Alder reactions of 1-oxa-1,3-butadienes: Synthesis of novel annelated pyrrolo [1, 2-a] indoles. *Tetrahedron Lett.* **2005**, *46*, 3391–3393. [[CrossRef](#)]
9. Tietze, L.F. Domino reactions in organic synthesis. *Chem. Rev.* **1996**, *96*, 115–136. [[CrossRef](#)]
10. Wan, J.P.; Jing, Y.; Liu, Y.; Sheng, S. Metal-free synthesis of cyano acrylates via cyanuric chloride-mediated three-component reactions involving a cascade consists of Knoevenagel condensation/cyano hydration/esterification. *RSC Adv.* **2014**, *4*, 63997–64000. [[CrossRef](#)]
11. Wang, H.J.; Liu, X.F.; Saliy, O.; Hu, W.; Wang, J.G. Robust Amino-Functionalized Mesoporous Silica Hollow Spheres Templated by CO₂ Bubbles. *Molecules* **2022**, *27*, 53. [[CrossRef](#)]
12. Ono, Y. Solid base catalysts for the synthesis of fine chemicals. *J. Catal.* **2003**, *216*, 406–415. [[CrossRef](#)]
13. Li, T.F.; Miras, H.N.; Song, Y.F. Polyoxometalate (POM)-Layered Double Hydroxides (LDH) Composite Materials: Design and Catalytic Applications. *Catalysts* **2017**, *7*, 260. [[CrossRef](#)]
14. Shanthan, R.P.; Venkataratnam, R.V. Zinc chloride as a new catalyst for Knoevenagel condensation. *Tetrahedron Lett.* **1991**, *32*, 5821–5822. [[CrossRef](#)]
15. Bartoli, G.; Beleggia, R.; Giuli, S.; Giuliani, A.; Marcantoni, E.; Massaccesi, M.; Paletti, M. The CeCl₃·7H₂O–NaI system as promoter in the synthesis of functionalized trisubstituted alkenes via Knoevenagel condensation. *Tetrahedron Lett.* **2006**, *47*, 6501–6504. [[CrossRef](#)]
16. Kubota, Y.; Nishizaki, Y.; Sugi, Y. High catalytic activity of as-synthesized, ordered porous silicate–quaternary ammonium composite for Knoevenagel condensation. *Chem. Lett.* **2000**, *29*, 998–999. [[CrossRef](#)]
17. Yokoi, T.; Yoshitake, H.; Tatsumi, T. Synthesis of amino-functionalized MCM-41 via direct co-condensation and post-synthesis grafting methods using mono-, di- and tri-amino-organoalkoxysilanes. *J. Mater. Chem.* **2004**, *14*, 951–957. [[CrossRef](#)]
18. Katkar, S.S.; Lande, M.K.; Arbad, B.R.; Rathod, S.B. Indium Modified Mesoporous Zeolite AlMCM-41 as a Heterogeneous Catalyst for the Knoevenagel Condensation Reaction. *Bull. Kor. Chem. Soc.* **2010**, *31*, 1301–1304. [[CrossRef](#)]
19. Ansari, M.B.; Jin, H.; Parvin, M.N.; Park, S.-E. Mesoporous carbon nitride as a metal-free base catalyst in the microwave assisted Knoevenagel condensation of ethylcyanoacetate with aromatic aldehydes. *Catal. Today* **2012**, *185*, 211–216. [[CrossRef](#)]
20. Reddy, T.I.; Verma, R.S. Rare-earth (RE) exchanged NaY zeolite promoted Knoevenagel condensation. *Tetrahedron Lett.* **1997**, *38*, 1721–1724. [[CrossRef](#)]
21. Grass, J.P.; Kluehspies, K.; Reiprich, B.; Schwieger, W.; Inayat, A. Layer-Like Zeolite X as Catalyst in a Knoevenagel Condensation: The Effect of Different Preparation Pathways and Cation Exchange. *Catalysts* **2021**, *11*, 474. [[CrossRef](#)]
22. Modak, A.; Mondal, J.; Bhaumik, A. Porphyrin based porous organic polymer as bi-functional catalyst for selective oxidation and Knoevenagel condensation reactions. *Appl. Catal. A Gen.* **2013**, *459*, 41–51. [[CrossRef](#)]
23. Bennazha, J.; Zahouilly, M.; Boukhari, A.; Hol, E.A. Investigation of the basis of catalytic activity of solid state phosphate complexes in the Knoevenagel condensation. *J. Mol. Catal. A Chem.* **2003**, *202*, 247–252. [[CrossRef](#)]
24. Karmakar, A.; Soliman, M.M.A.; Alegria, E.C.B.A.; Guedes da Silva, M.F.C.; Pombeiro, A.J.L. Polyaromatic Carboxylate Ligands Based Zn(II) Coordination Polymers for Ultrasound-Assisted One-Pot Tandem Deacetalization–Knoevenagel Reactions. *Catalysts* **2022**, *12*, 294. [[CrossRef](#)]
25. Gascon, J.; Aktay, U.; Hernandez-Alonso, M.D.; Klink, G.P.M.; Kapteijn, F. Amino-based metal-organic frameworks as stable, highly active basic catalysts. *J. Catal.* **2009**, *261*, 75–87. [[CrossRef](#)]
26. Hartmann, M.; Fischer, M. Amino-functionalized basic catalysts with MIL-101 structure. *Microporous Mesoporous Mater.* **2012**, *164*, 38–43. [[CrossRef](#)]
27. Lin, R.; Ding, Y. A Review on the Synthesis and Applications of Mesostructured Transition Metal Phosphates. *Materials* **2013**, *6*, 217–243. [[CrossRef](#)]

28. Loiseau, T.; Ferey, G. Crystalline oxyfluorinated open-framework compounds: Silicates, metal phosphates, metal fluorides and metal-organic frameworks (MOF). *J. Fluor. Chem.* **2007**, *128*, 413–422. [[CrossRef](#)]
29. Wilson, S.T.; Lok, B.M.; Messina, C.A.; Cannan, T.R.; Flanigen, E.M. Aluminophosphate Molecular Sieves: A New Class of Microporous Crystalline Inorganic Solids. *J. Am. Chem. Soc.* **1982**, *104*, 1146–1147. [[CrossRef](#)]
30. Pyke, D.R.; Whitney, P.; Houghton, H. Chemical modification of crystalline microporous aluminium phosphates. *Appl. Catal.* **1985**, *18*, 173–190. [[CrossRef](#)]
31. Ramesha, B.M.; Meynen, V. Advances and Challenges in the Creation of Porous Metal Phosphonates. *Materials* **2020**, *13*, 5366. [[CrossRef](#)]
32. Clearfield, A. Recent advances in metal phosphonate chemistry. *Curr. Opin. Solid State Mater. Sci.* **1996**, *1*, 268–278. [[CrossRef](#)]
33. Fischer, M. Porous aluminophosphates as adsorbents for the separation of CO₂/CH₄ and CH₄/N₂ mixtures—A Monte Carlo simulation study. *Sustain. Energy Fuels* **2018**, *2*, 1749–1763. [[CrossRef](#)]
34. Nan, C.; Lu, J.; Chen, C.; Peng, Q.; Li, Y. Solvothermal synthesis of lithium iron phosphate nanoplates. *J. Mater. Chem.* **2011**, *21*, 9994–9996. [[CrossRef](#)]
35. Wang, H.Y.; Cheng, H.J.; Lai, F.; Xiong, D.Y. CuAPO-5 as a Multiphase Catalyst for Synthesis of Verbenone from alpha-Pinene. *Materials* **2022**, *15*, 8097.
36. Xu, D.; Ren, J.; Yue, S.; Zou, X.; Shang, X.; Wang, X. One-Pot Synthesis of Al-P-O Catalysts and Their Catalytic Properties for O-Methylation of Catechol and Methanol. *Materials* **2021**, *14*, 5942. [[CrossRef](#)]
37. Cheng, S.; Tzeng, J.N.; Hsu, B.Y. Synthesis and Characterization of a Novel Layered Aluminophosphate of Kanemite-like Structure. *Chem. Mater.* **1997**, *9*, 1788–1796.
38. Lok, B.M.; Messina, C.R.; Patton, R.L.; Gajek, R.T.; Cannan, T.R.; Flanigan, E.M. Silicoaluminophosphate molecular sieves: Another new class of microporous crystalline inorganic solids. *J. Am. Chem. Soc.* **1984**, *106*, 6092–6093. [[CrossRef](#)]
39. Zubowa, H.L.; Richter, M.; Roost, U.; Parltitz, B.; Fricke, R. Synthesis and catalytic properties of substituted AlPO₄-31 molecular sieves. *Catal. Lett.* **1993**, *19*, 67–79.
40. Sayari, A.; Moudrakovski, I.; Reddy, J.S.; Ratcliffe, C.I.; Ripmeester, J.A.; Preston, K.F. Synthesis of mesostructured lamellar aluminophosphates using supramolecular templates. *Chem. Mater.* **1996**, *8*, 2080–2088. [[CrossRef](#)]
41. Lin, X.X.; Su, M.X.; Fang, F.X.; Hong, J.F.; Zhang, Y.M.; Zhou, S.F. Hierarchically Annular Mesoporous Carbon Derived from Phenolic Resin for Efficient Removal of Antibiotics in Wastewater. *Molecules* **2022**, *27*, 6735. [[CrossRef](#)]
42. Dutta, A.; Patra, A.K.; Bhaumik, A. Porous organic–inorganic hybrid nickel phosphonate: Adsorption and catalytic applications. *Microporous Mesoporous Mater.* **2012**, *155*, 208–214. [[CrossRef](#)]
43. Thakkar, R.; Chudasama, U. Preparation and application of zirconium phosphate and its derivatives. *J. Hazard. Mater.* **2009**, *172*, 129–133. [[CrossRef](#)]
44. Ge, T.D.; Yu, L.Q.; Ni, N.R.; Dong, T.A.; Xing, T.L.; Long, H.K.; Yang, J.X. Synthesis of LiCo_{1/3}Ni_{1/3}Mn_{1/3}O₂ as a cathode material for lithium ion battery by water-in-oil emulsion method. *Mater. Chem. Phys.* **2005**, *94*, 423–428.
45. Altomare, A.; Cuocci, C.; Giacobozzo, C.; Moliterni, A.; Rizzi, R.; Corriero, N.; Falcicchio, A. EXPO2013: A kit of tools for phasing crystal structures from powder data. *J. Appl. Crystallogr.* **2013**, *46*, 1231–1235. [[CrossRef](#)]
46. Chakroborty, D.; Chowdhury, A.; Chandra, M.; Jana, R.; Shyamal, S.; Bhunia, M.K.; Chandra, D.; Hara, M.; Pradhan, D.; Datta, A.; et al. Novel Tetradentate Phosphonate Ligand Based Bioinspired Co-Metal–Organic Frameworks: Robust Electrocatalyst for the Hydrogen Evolution Reaction in Different Mediums. *Cryst. Growth Des.* **2021**, *21*, 2614–2623. [[CrossRef](#)]
47. Kundu, S.K.; Bhaumik, A. Pyrene-Based Porous Organic Polymers as Efficient Catalytic Support for the Synthesis of Biodiesels at Room Temperature. *ACS Sustain. Chem. Eng.* **2015**, *3*, 1715–1723. [[CrossRef](#)]
48. Zhang, W.; Oulego, P.; Sharma, S.K.; Yang, X.-L.; Li, L.-J.; Rothenberg, G.; Shiju, N.R. Self-Exfoliated Synthesis of Transition Metal Phosphate Nanolayers for Selective Aerobic Oxidation of Ethyl Lactate to Ethyl Pyruvate. *ACS Catal.* **2020**, *10*, 3958–3967. [[CrossRef](#)]
49. Sharma, N.; Parhizkar, M.; Cong, W.; Mateti, S.; Kirkaland, M.A.; Puri, M.; Sutti, A. Metal ion type significantly affects the morphology but not the activity of lipase–metal–phosphate nanoflowers. *RSC Adv.* **2017**, *7*, 25437–25443. [[CrossRef](#)]
50. Li, Z.; Tang, M.; Dai, J.; Wang, T.; Wang, Z.; Bai, W.; Bai, R. Preparation of Covalent Pseudo-Two-Dimensional Polymers in Water by Free Radical Polymerization. *Macromolecules* **2017**, *50*, 4292–4299. [[CrossRef](#)]
51. Mazzotta, M.G.; Gupta, D.; Saha, B.; Patra, A.K.; Bhaumik, A.; Abu-Omar, M.M. Efficient Solid Acid Catalyst Containing Lewis and Bronsted Acid Sites for the Production of Furfurals. *ChemSusChem* **2014**, *7*, 2342–2350. [[CrossRef](#)]
52. Farhi, J.; Lykakis, I.N.; Kostakis, G.E. Metal-Catalysed A(3) Coupling Methodologies: Classification and Visualisation. *Catalysts* **2022**, *12*, 660. [[CrossRef](#)]
53. Tan, Y.; Fu, Z.; Zhang, J. A layered amino-functionalized zinc-terephthalate metal organic framework: Structure, characterization and catalytic performance for Knoevenagel condensation. *Inorg. Chem. Commun.* **2011**, *14*, 1966–1970. [[CrossRef](#)]
54. Hwang, Y.K.; Hong, D.-Y.; Chang, J.-S.; Jhung, S.H.; Seo, Y.-K.; Kim, J.; Vimont, A.; Daturi, M.; Serre, C.; Ferey, G. Amine grafting on coordinatively unsaturated metal centers of MOFs: Consequences for catalysis and metal encapsulation. *Angew. Chem. Int. Ed.* **2008**, *47*, 4144–4148. [[CrossRef](#)] [[PubMed](#)]

55. Das, A.; Anbu, N.; Dhakshinamoorthy, A.; Biswas, S. A highly catalytically active Hf(IV) metal-organic framework for Knoevenagel condensation. *Microporous Mesoporous Mater.* **2019**, *284*, 459–467. [[CrossRef](#)]
56. Basavaraja, D.; Athira, C.S.; Siddalingeshwar, V.D.; Ashitha, K.T.; Somappa, S.B. Multicomponent Synthesis of Spiro-dihydropyridine Oxindoles via Cascade Spiro-cyclization of Knoevenagel/Aza-Michael Adducts. *J. Org. Chem.* **2022**, *87*, 13556–13563.

Disclaimer/Publisher's Note: The statements, opinions and data contained in all publications are solely those of the individual author(s) and contributor(s) and not of MDPI and/or the editor(s). MDPI and/or the editor(s) disclaim responsibility for any injury to people or property resulting from any ideas, methods, instructions or products referred to in the content.